International Journal of Engineering and Science Invention (IJESI)
ISSN (Online): 2319-6734, ISSN (Print): 2319-6726
www.ijesi.org ||Volume 14 Issue 4 April 2025 || PP 152-159

Measurement of Switching Surges and Resonance Behaviour in Transformer Windings

Pinkal Kumar[1], Prof. Abhishek Kaushik[2]
Scholar M.Tech(E.E) VGI[1] , HOD Dept. of EE, VGI[2]
tyagipinkal01@gmail.com [1], abhishek.kaushik@vgi.ac.in [2]

Abstract: *Internal wrapping vibration is a phenomenon that can cause excess voltage within transformer windings. This research will use Multi-conductor Transmission Line (MTL) model to investigate resonance behaviour in transformers winds. The MTL model is used to control which turns might cause wadding failure owing to interior zigzagging characters. Because an internal circuit oscillation can be triggered when the frequency of an incoming outpouring meets the transformer's resonance range, we measured the switching surges produced when switching a power supply with a dry circuit breaker. The results of the pre-strike behavior also suggested a high du/dt, which might lead to straining of generator's end turn wadding.*

Key words: *MTL model, pre-strike, resonance over-voltage.*

I. Introduction

Swapping transients caused by emptiness circuit waves can induce booming overvoltage's in step-up modernizers used in wind turbines. In medium-voltage systems, operation of space circuit waves often leads to phenomena such as pre-strikes and re-ignitions, which generate high-frequency oscillations accompanied by steep voltage gradients (high du/dt). These conditions impose significant stress on the transformer's end-turn wadding. One of the more critical issues arising from this is resonance within the transformer windings, which may be categorized as either interior or outside.

External character typically results from the interaction between the transformer and connected cables. This occurs when natural frequency of cable aligns with transformer's natural occurrence, often observed in wind turbine applications. In such systems, energizing the transformer can trigger resonant transients due to this cable-transformer interaction. Onshore wind farms, in particular, may use extensive cabling—up to 600 meters long—where quarter-wave frequency of the hawsers can coincide with the resonant frequencies of the transformer. This overlap may cause overvoltages at the low-voltage terminals of the step-up transformers and within the high-voltage windings. Internal resonance takes place when a specific frequency within a surge coincides with a resonance frequency of the transformer's winding. This scenario can lead to severe internal overvoltages, possibly causing flashovers between windings or from the winding to the core. However, internal resonances do not always result in direct failure; they may initiate partial discharges, which gradually degrade the insulation and ultimately lead to breakdown. Detecting these resonant overvoltages is challenging because they occur inside the windings and not at the terminals. As such, specialized prototype transformers or advanced high-frequency transformer models are used for assessment. In poetry, two main high-frequency modeling systems are used: the Multi-Conductor Transmission Line (MTL) model and the RLC ladder network. The MTL model is generally applied for analyzing fast transients with frequency machineries above 1 MHz, where the RLC ladder circuit is more suitable for transients up to 1 MHz.

A study in [9] explored resonant overvoltages using a custom-built prototype step-down transformer rated at 11/0.24 kV and 500 kVA. This transformer was constructed with three distinct winding configurations: pancake, layer, and disc. The findings indicated that layer windings tended to transfer higher overvoltages to the low-voltage terminals compared to the other designs. Nevertheless, both layer and pancake windings exhibited lower internal resonance overvoltages than the disc winding.The focus of this work is to compute inter-turn overvoltages based on modernizer limitations sourced from [6] and to analyze switching transient measurements collected from an operational wind farm.

II. Background:

Voltage circulation across modernizer windings can be modeled using a network of consistent and mutually attached program lines, as illustrated in Fig1.

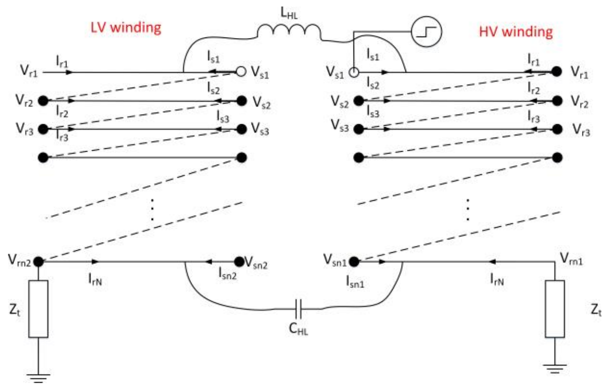

Figure 1: Multi-conductor Transmission Line model

Fig1 illustrates a modeled symbol of the high-voltage (HV) and low-voltage (LV) winds. According to SANS 60076-3, the powers transferred between these windings exhibit both capacitive and inductive properties. These characteristics are represented in Figure 1 by CHL (capacitance) and LHL (inductance), respectively. Interaction between the coupled broadcast appearances can be designated using Telegrapher's equations, as shown in Equ 1 and Equ 2.

$$\frac{d^2\mathbf{V}}{d\mathbf{x}^2} = -[Z][Y] \qquad (1)$$

$$\frac{d^2\mathbf{I}}{d\mathbf{x}^2} = -[Z][Y] \qquad (2)$$

Let **V** and III represent the vectors of occurrence power and present, individually. The matrices **Z** and **Y** correspond to the line's impedance and admittance. By solving the Telegrapher's equations, the voltage and current at a given point xxx along the line can be determined, as illustrated in Equations (3) and (4) [10].

$$V_x = V_1 e^{-[P]x} + V_2 e^{[P]x} \qquad (3)$$

$$I_x = Y_o \quad V_1 e^{-[P]x} - V_2 e^{[P]x} \qquad (4)$$

By smearing borderline situations to solutions of Equations 3 and 4, the voltages at sending end (S) and getting end (R) can be derived, as represented in Equ 5 [6].

$$\begin{bmatrix} I_S \\ I_R \end{bmatrix} = \begin{bmatrix} A & -B \\ -B & A \end{bmatrix} \begin{bmatrix} V_S \\ V_R \end{bmatrix} \qquad (5)$$

where:

$$A = YS\gamma^{-1}\coth(\gamma l)\,S^{-1} \qquad (6)$$

$$B = YS\gamma^{-1}\mathit{cosech}(\gamma l)\,S^{-1} \qquad (7)$$

IR and IS represent current vectors at receiving and distribution ends, correspondingly, while VR and VS denote power vectors at getting and transport ends. In Equations 6 and 7, **S** refers to the eigenvector matrix, and **γ^2** represents the eigenvalue matrix derived from the product of matrices Z and Y. The variable **l** signifies the line length. Upon further simplification of Equation 5, the following expression is obtained:

$$\begin{bmatrix} I_{S1} \\ I_{S2} \\ \cdot \\ \cdot \\ I_{Sn} \\ I_{R1} \\ I_{R2} \\ \cdot \\ \cdot \\ I_{RN} \end{bmatrix} = \begin{bmatrix} A & -B \\ -B & A \end{bmatrix} \begin{bmatrix} V_{S1} \\ V_{S2} \\ \cdot \\ \cdot \\ V_{Sn} \\ V_{R1} \\ V_{R2} \\ \cdot \\ \cdot \\ V_{RN} \end{bmatrix} \qquad (8)$$

Based on Figure 1, the following identities can be utilized in relation to Equation 8 [1

$$I_{r1} = -I_{s2} \qquad I_{r2} = -I_{s3} \qquad -I_{rn} = V_{rn}/Z_t \qquad V_{r1} = V_{s2}$$
$$V_{r2} = V_{s3} \qquad \ldots$$

This allows the use of matrix reduction techniques without modifying the system equations, leading to the formulation shown in Equation 9

$$\begin{bmatrix} I_{S1} \\ 0 \\ \cdot \\ \cdot \\ 0 \\ 0 \end{bmatrix} = \begin{bmatrix} & & \\ & Y & \\ & & \end{bmatrix} \begin{bmatrix} V_{S1} \\ V_{S2} \\ \cdot \\ \cdot \\ V_{Sn} \\ V_{Rn} \end{bmatrix} \qquad (9)$$

Let **Y** represent an **n × n** matrix. In Figure 1, the termination impedance ZtZ_tZt of the transformer winding is considered to be 10−9 Ω10^{-9} \ \Omega10−9 Ω [12]. By removing the current IS1I_{S1}IS1 from Equ 9, the calculation can be reformulated as Equ10, which enables the calculation of voltages at any selected turn k.

$$\begin{bmatrix} V_{S2} \\ V_{S3} \\ \cdot \\ \cdot \\ V_{Sn} \end{bmatrix} = \begin{bmatrix} H_1 & & \\ H_2 & & \\ \cdot & & \\ \cdot & & \\ H_{n-1} & & \end{bmatrix} \begin{bmatrix} V_{S1} \\ 0 \\ \cdot \\ \cdot \\ 0 \end{bmatrix} \qquad (10)$$

Magnitude of transfer meaning at iteration k, relative to the effort, can be determined as described in [5]:

$$H_k = \frac{YY_{(k+1,1)}}{YY_{(1,1)}} \qquad k = 1, 2, \cdots, n-1 \qquad (11)$$

Y represents the inverse of matrix Y as defined in Equ9, and H is a square matrix with dimensions (n-1) x (n-1). It is important to clarify that this paper does not concentrate on the surge transmission from the high-voltage (HV) winding to the low-voltage (LV) winding, as illustrated in Figure 1.

III. PARAMETER CALCULATION OF A TRANSFORMER WINDING:

Liang, in references [6] and [13], presented a method for modeling transformer windings to examine resonant overvoltage phenomena. The study utilized a core-type convertor, and the winding parameters listed in Table 1 from reference [13] are adopted in this paper. The impedance and entrance matrices, represented respectively as **Z=R+jωL** and **Y=G+jω C** are determined based on Equations (1) and (2).

$$Z = \left[j\omega\mathbf{L} + \left(\frac{1}{2(d_1 + d_2))} \right) \cdot \sqrt{\frac{\pi f \mu}{\sigma}} \right] \quad (12)$$

$$Y = (j\omega + \omega \tan\delta)\, \mathbf{C} \quad (13)$$

In this context, μ represents the permeability and σ denotes the conduction of the conductor, while d_1 and d_2 refer to the conductor's diameters

Table 1: Main Parameters of the winding

Number Of discs	18
Turns per disc	10
Conductor width [mm]	6.95
Conductor height [mm]	11.2
Average turn length [m]	1.4828
Thickness of inter-turn insulation [mm]	3.00
Relative permittivity of inter-turn insulation	3.5
Conductor conductance [s $\cdot m^{-1}$]	$3x10^7$
Inter-turn capacitance (C_k) [pF $\cdot m^{-1}$]	120
Inter-section capacitance (C_s) [pF $\cdot m^{-1}$]	10
Turn to core capacitance (C_g) [pF $\cdot m^{-1}$]	15

In Equation (12), the real component accounts for the skin effect observed at elevated frequencies [13]. Meanwhile, the real component in Equation (13) corresponds to the dissipation factor (tan δ), which represents dielectric losses [5], [12]. It is important to recognize that tan δ varies with frequency, moisture content, and temperature, significantly affecting the admittance matrix at higher frequencies. To capture the frequency-dependent behavior of transformer insulation, an approximate expression for tan δ, given in Equation (14), was utilized [3].

$$tan(\delta) = (1.082x10^{-8}) \cdot 2\pi f + 5.0x10^{-3} \quad (14)$$

The matrices for condenser and inductor were determined using the following method:

3.1 *Capacitance*

The capacitance matrix C was constructed as described in [12] with the following characteristics:
- $C_{i,i}$ capacitance of layer i to ground and the sum of all other capacitances connected to layer i
- $C_{i,j}$ capacitances between layers i and j taken with negative sign ($i \neq j$)

It is important to highlight that the capacitance matrix plays a vital role in accurately determining the transient voltage differences between winding turns.

3.2 Inductance

The inductance matrix can be derived in two components. The first component is obtained directly from the capacitance matrix **C**, provided that the following assumptions are satisfied [11]:
- The penetration of high-frequency magnetic flux into the iron laminations and the transformer core is minimal.
- The magnetic flux remains confined within the insulated pathways.

Using Equation 15, the initial inductance matrix can be derived.

$$L_n = \frac{\varepsilon_r}{v^2} \cdot \mathbf{C}^{-1} \quad (15)$$

Here, v represents the speed of light in a vacuum, and εr denotes the relative permittivity of the insulating material, which, in this context, is the effective permittivity resulting from the combination of air and paper. The second component of the inductance accounts for the magnetic flux within the conductor itself [13]. It is expressed as:

$$L_i = \frac{\mathbf{R}}{f} \qquad (16)$$

where **R** represents the real component of Equation 12. The complete inductance matrix can be formulated as:

$$\mathbf{L} = L_n + L_i \cdot E_n \qquad (17)$$

where E_n is a unit matrix of size nxn.

IV. COMPARISON WITH PREVIOUS WORK

As previously indicated, the research conducted by Liang in [6] and [13] served as the foundation for this study. The purpose of replicating Liang's work was to confirm the accuracy of the original findings and assess the effectiveness of the proposed algorithm. Following this, the algorithm is intended to be applied to wind farm transformers to investigate whether failures might be linked to resonance effects. Resonance in transformer windings typically occurs when the frequency components of switching surges align with one of the winding's natural resonant frequencies. These high-frequency components can compromise insulation integrity, often resulting in breakdowns near the lead-in end of the windings [13].

Figure 2: Magnitude of the transfer function of turn 20 relative to the input

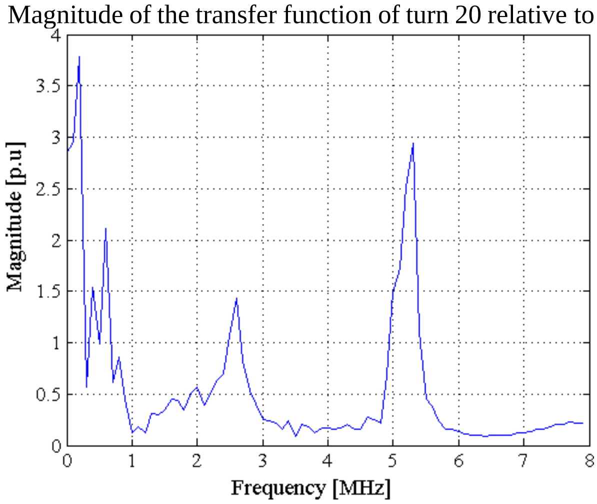

Figures 2, 3, and 4 illustrate the magnitude profiles observed at various turns of the transformer winding. A key observation from these waveforms is that the amplitude of high-frequency components tends to diminish as the number of turns increases along the winding. The waveforms indicate a resonant frequency occurring in the range of approximately 5 to 6 MHz. When compared to the findings presented by Liang in [13], a similar overall waveform pattern is evident, although some discrepancies in the amplitude of specific frequency components exist. These variations may be attributed to assumptions made during the calculation of the loss tangent, tan(δ), and the use of an estimated termination impedance value of Zt = 10^{-9} Ω. Nevertheless, the data presented in Figures 2 through 4 serve as a reliable approximation for analyzing resonance behavior in transformer windings and assessing the potential for inter-turn insulation failure

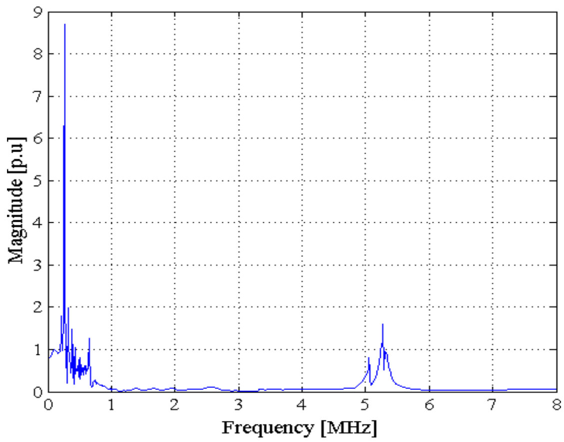

Figure 3: Magnitude of the transfer function of turn 40 relative to the input

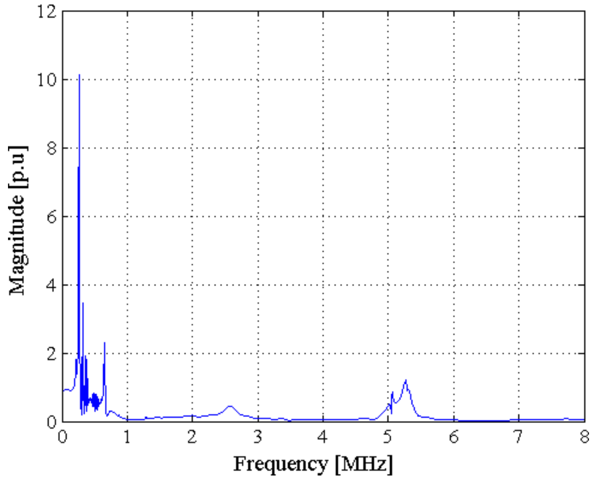

Figure 4: Magnitude of the transfer function of turn 60 relative to the input

4.1 Measurement of switching transients

As previously mentioned, internal resonance arises when a component of the incoming surge frequency aligns with the natural resonance frequency of the transformer winding. To investigate this phenomenon, switching transient tests were performed on a wind turbine transformer. These tests included:

1. Energizing the transformer under no-load conditions.
2. Disconnecting the transformer while it remained under no-load.

Phase-to-earth voltages across the three medium voltage (MV) phases were recorded using capacitive voltage dividers connected to each phase. The MV bushing screen exhibited a measured capacitance of 32 pF, and an external 10 nF capacitor was connected in series between the bushing screen terminal and the transformer tank, which served as the local ground. This setup produced a voltage division ratio of 313. The measurement configuration, with the FLUKE 1750 device connected to the phase conductors, is illustrated in Figure 5.

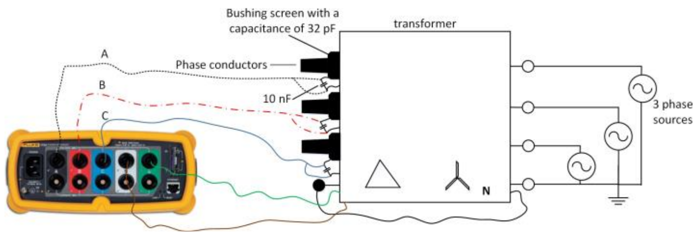

Figure 5: Measurement setup for recording transients

4.2 *Energizing the transformer during no-load*

Energizing a transformer consistently leads to at least one pre-strike event in each phase [14]. When a vacuum circuit breaker closes, it can cause high rate-of-change-of-voltage (du/dt) transients at the transformer terminals, resulting in overvoltages occurring within a few milliseconds [15]. This phenomenon is evident from the transient

measurements shown in Figure 6. The waveform analysis in Figure 6 indicates the presence of pre-strike activity accompanied by a rapid du/dt, which may trigger resonance overvoltages inside the transformer windings.
The following scenarios were considered:

1. Energizing the transformer under no-load conditions.
2. Disconnecting the transformer while it is under no-load.

To measure the medium-voltage (MV) phase-to-earth voltages for all three phases, capacitive voltage dividers were employed on each phase. The MV bushing screen exhibited a capacitance of 32 pF, and an additional 10 nF capacitor was connected externally in series between the bushing screen terminal and the transformer tank, which served as a local earth reference. This setup produced a voltage division ratio of 313. Figure 5 illustrates the measurement arrangement with the FLUKE 1750 connected to the phase conductors.

4.3 Disconnecting the transformer during no-load

When the VCB (Vacuum Circuit Breaker) disconnects, excessive over-voltages may arise if the arc reignites following the initial interruption of current [16]. If the VCB fails to extinguish the arc effectively, multiple reignitions can take place, causing the voltage to rise with each occurrence and leading to increased over-voltages. However, no notable over-voltages were observed when the transformer was de-energized.

V. DISCUSSION :

This paper explores the phenomenon of resonant overvoltages. Traditional white-box models, such as the MTL and RLC models, require detailed knowledge of the transformer winding geometry. Since the exact parameters of the wind turbine transformers were unavailable, this study utilized external transformer parameters to demonstrate resonance effects in transformer windings. However, the model has certain limitations. For instance, a predefined termination impedance value was assumed. As noted in [12], to prevent computational divergence, a very small impedance, $Z_t = 10^{-9}\ \Omega$, is necessary. This value may differ from the termination impedance employed by Liang in [6], [13]. Furthermore, as discussed earlier, tan(δ) depends on frequency, moisture content, and temperature, and Equation 14 provides only an approximation. Therefore, at frequencies exceeding 1 MHz, Equation 14 does not accurately reflect the complex frequency dependence of the dissipation factors in transformer insulation, which is essential for precise modeling with the MTL model [3].

The next topic that requires attention is the calculation of resistance. In [13], Liang determined the resistance by incorporating the skin effect that occurs at high frequencies, as illustrated in Equation 12. Alternatively, Equation 18 presents a different method for computing the impedance.

$$Z = \left(j\omega + \sqrt{\frac{2\omega}{\sigma \mu_o d^2}} \right) L \qquad (18)$$

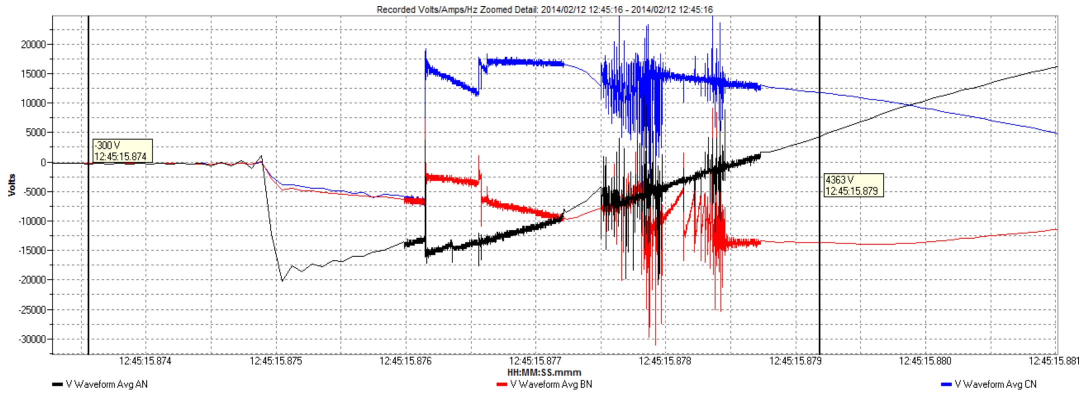

Figure 6: Measured pre-strike behavior on closing of the vacuum circuit breaker

The real component considers both the skin effect and the proximity effects in the conductor, which vary depending on frequency [12]. In Equation (18), **d** represents the spacing between layers, while **σ** denotes the conductor's conductivity. As reported in [3], the total resistance is primarily influenced by the proximity effect when frequencies exceed 4 MHz. Ignoring proximity effects, as done by Liang in [13], and only accounting for the skin effect in resistance calculations can lead to resonance frequencies below 1 MHz exhibiting significantly high amplitudes [3], as demonstrated in Figures 2, 3, and 4. To support Hans Kristian Hidalen's observation [3], the transfer function magnitude at the 20th turn was recalculated including the proximity effect. The outcomes of the multi-turn line (MTL) model, using the impedance defined in Equation (18), are displayed in Figure 7. Analysis of this figure reveals that the previously prominent resonance peaks below 1 MHz have been substantially reduced in amplitude when compared to the original waveform shown in Figure 2. Not taking into account the proximity effects can lead to calculated results which have a poor agreement with measurements as shown in [3].

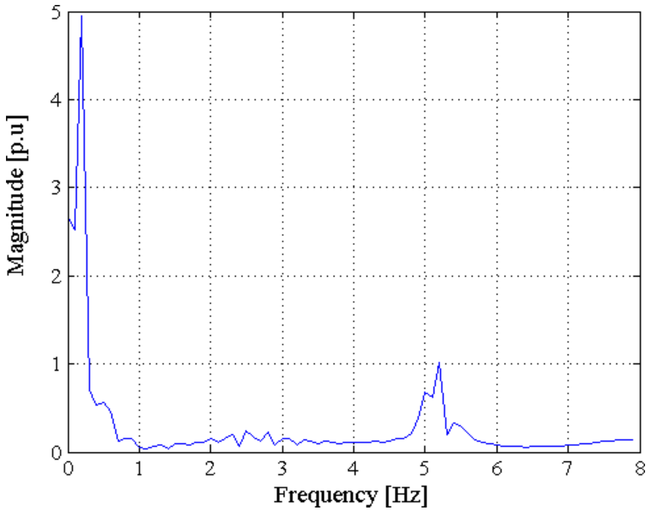

Figure 7: Magnitude of transfer function of turn 20 relative to the input (taking into account proximity effects)

VI. Concussion:

This paper discusses resonance effects in transformer windings and examines the measurement of switching transients. The MTL model is employed to estimate the magnitude of resonant over-voltages occurring between turns, as well as the potential for turn-to-turn breakdown. While the model has some limitations, the close qualitative correlation between the simulated waveforms and the experimental data provides valuable insights into the internal winding resonance behavior in transformers.

References:

[1]. T. Craenenbroek, J. D. Ceuster, J. P. Marly, H. D. Herdt, B. Brouwers, and D. V. Dommelen. "Experimental and numerical analysis of fast transient phenomena in distribution transformers." *in IEEE Power Engineering Society Winter Meeting, Singapore*, vol. 3, no. 1, pp. 2193–2198, Jan. 2000.

[2]. M. Popov and L. van der Sluis. "Improved calculations for no-load transformer switching surges." *in IEEE Transactions on Power Delivery*, vol. 16, no. 3, pp. 401–408, Jan. 2001.

[3]. H. Soloot, H. K. Hidalen, and B. Gustavsen. "Modeling of Wind Turbine Transformers for the Analysis of Resonant Overvoltages." *in International Conference on Power Systems Transients IPST2013 in Vancouver, Canada*, pp. 1–7, Jul. 2013.

[4]. M. Popov, L. V. der Sluis, G. C. Paap, and H. D. Herdt. "Computation of Very Fast Transient Overvoltages in Transformer Windings." *in IEEE Transactions on POWER DELIVERY*, vol. 18, no. 4, pp. 1268–1274, Oct. 2003.

[5]. M. Popov, L. V. der Sluis, R. P. P. Smeets, and J. L. Roldan. "Analysis of Very Fast Transients in *Layer − Type* Transformer Windings." *in IEEE TRANSACTIONS ON POWER DELIVERY*, vol. 22, no. 1, pp. 238–247, Jan. 2007.

[6]. H. Sun, G. Liang, X. Zhang, and X. Cui. "Analysis of Resonance in Transformer Windings under Very Fast Transient Overvoltages." *in 17th International Zurich Symposium on Electromagnetic Compatibility*, vol. 22, no. 1, pp. 432–435, Jan. 2006.

[7]. J. Du, G. Liang, H. Sun, X. Liu, and X. Liu. "Lumped Parameter Modeling of Transformer windings under VFTO." *in 17th International Zurich Symposium on Electromagnetic Compatibility*, pp. 258–261, Jan. 2011.

[8]. S. Hosseini, M. Vakilian, and G. Gharehpetian. "Comparison of transformer detailed models for fast and very fast transient studies." *in IEEE Transactions on Power Delivery*, vol. 23, no. 2, pp. 733–741, Apr. 2008.

[9]. H. Soloot, H. K. Hidalen, and B. Gustavsen. "Upon the Improvement of the Winding Design of Wind Turbine Transformers for Safer Performance within Resonance Overvoltages." *in Tenth Deep Sea Offshore Wind Research and Development Seminar*, pp. 1–7, Jan. 2013.

[10]. S. N. Hettiwatte, P. A. Crossley, Z. D. Wang, Darwin, and G. Edwards. "Simulation of a transformer winding for partial discharge propagation studies." *in IEEE Power Engineering Society Winter Meeting*, vol. 2, no. 1, pp. 95–101, Jun. 2002.